Digital beamforming antenna array with polarisation multiplexing for mobile high-speed satellite terminals at Ka-band

Benjamin Rohrdantz[1], Karsten Kuhlmann[2], Alexander Stark[3], Alexander Geise[4], Arne F. Jacob[1]

[1]*Institut für Hochfrequenztechnik, Technical University of Hamburg-Harburg, 21073 Hamburg, Germany*
[2]*Physikalisch-Technische Bundesanstalt (PTB), Hochfrequenzmesstechnik, 38116 Braunschweig, Germany*
[3]*OHB System AG, 28359 Bremen, Germany*
[4]*Airbus Defense and Space GmbH, Compact Range & Test Services, 82024 Taufkirchen, Germany*
E-mail: benjamin.rohrdantz@tuhh.de

Abstract: In this contribution, a planar antenna array terminal for mobile satellite communications at Ka-band is proposed. This Earth station on mobile platform uses separate transmit and receive apertures to obtain a flat design well suited for aeronautical applications. Digital beamforming is applied for fast beam scanning, tracking, and enhanced post-processing capabilities. The active antenna elements exhibit dual polarisation to comply with a four-colour spot beam arrangement commonly used by high-throughput satellites. Advanced frontend packaging concepts for a high integration density enable half wavelength element spacing. This prevents grating lobes and yields a large scanning range. A modular approach allows to flexibly adapt the array size to the application specific needs. An 8×8 receiver (Rx) array at 20 GHz and a 16×3 transmitter array at 30 GHz are demonstrated. The measured results obtained in conjunction with inter-element decoupling validate the approach. The principal suitability of the Rx array for the intended application is tested in a field experiment.

1 Introduction

Wireless communications have undergone a rapid development in the past decades. Driven by the progressing usage of mobile computers and smartphones around the globe, a necessity for wireless connections and Internet anywhere we work and live has evolved [1]. In densely populated areas, this can easily be met by wireless fidelity, third generation (3G)-, and 4G-networks. In rural and remote areas, supplying terrestrial Internet connections gets increasingly complex and ultimately fails on the oceans. Hence, satellite service providers such as iridium and Inmarsat offer worldwide L-band voice and data communication services [2, 3]. However, these are expensive and do not provide the required data rates for modern services such as video streaming.

Today, high-throughput satellites (HTSs) such as Intelsat Epic[NG] [4] at Ku-band (downlink 10.7-12.7\,GHz, uplink: 12.75-17.8\,GHz) and KA-Sat [5] at Ka-band (downlink 17.7-21.2\,GHz, uplink: 27.5-31.0\,GHz) offer viable solutions with their larger available bandwidth. Additionally, a multitude of narrow spot beams is employed to allow for spatial frequency reuse and thereby an even higher available data rate per satellite. Neighbouring spot beams are arranged according to the four-colour theorem [6] to minimise interference. The colours are represented through two frequency and two polarisation states. The offered capacity is high and affordable enough to compete with fixed-broadband services [7].

HTS were originally constructed and are commonly used in conjunction with stationary terminals as a fixed satellite service. However, mobile Internet access, e.g. on-board aircrafts, ships, and trains, has become increasingly important. For these cases, a ground-based solution for continental flights is offered through Aircell, while Panasonic Avionics and Row 44 rely on Ku-band satellite-based coverage [8]. Airlines have a big interest to provide Internet connectivity for a convenient flight and an increased competitiveness, e.g. through free Internet access [9]. However, because of platform movements, a tracking and steering mechanism is required to point the antenna beam toward the satellite. Common solutions are complex mechanically steerable reflector antennas [10, 11]. These are however bulky and increase the drag and operational cost of aircrafts.

The alternative is electronic beam scanning using array antennas. They offer low-profile and instantaneous scanning as no moving parts are involved. Different commercial systems are currently under development by PHASOR Inc., Kymeta Corporation and a cooperation of Panasonic Avionics and Boeing Network and Space Systems. For the beam scanning, different techniques are used such as classical phase shifters [12] or tunable metamaterials [13, 14]. Recently, the technically more advanced concept of digital beamforming (DBF) has attracted considerable attention for communication at Ka-band frequencies and various solutions have been proposed [15–18].

This paper presents a low-profile antenna terminal for mobile satellite communications at Ka-band which makes use of DBF for inertia-free beam scanning in combination with advanced algorithms for improved performance. This paper is structured as follows. Section 2 introduces the reference scenario, the system design, and the benefits of DBF. In Section 3, the receiver (Rx) system is investigated in detail and the measurement results are presented. The design and performance of the transmit array are reported in Section 4. Section 5 summarises the performance of the proposed antenna system.

2 Array system design

Earth stations on mobile platforms (ESOMPs) are in great demand today to enable Internet access by HTS on-board mobile vehicles. This paper investigates an electronically scanned array for aeronautical applications at Ka-band. Owing to the large difference between the downlink (20 GHz) and uplink (30 GHz) frequencies and to relieve the packaging density Rx and transmitter (Tx) are realised with separate antennas. These are built from modules as this eases fabrication and serviceability, and allows the final antenna size to be flexibly adapted to different system requirements. Modules with 16 elements were found to be adequate.

2.1 Reference scenario

Ka-band satellite service availability has been steadily rising in the last decade. However, most services are geographically restricted to specific areas, so that no worldwide coverage is possible. Table 1 lists HTSs mainly at Ka-band frequencies, aside their coverage area and number of spot beams. Most of them operate in the

Table 1 HTS satellites and their coverage area

Satellite	Coverage area	Beams per Sat	Launch
Inmarsat-5 Global Xpress	quasi-global	89×3 Sat.	2014
Telenor THOR 7	European Shipping Routes	26	2015
O3b Networks ($8\times$)	Equatorial Regions	12×8 Sat.	2015
Viasat Anik F2	North America	38	2004
Avanti Hylas 1-2	Europe, Africa, Middle East	12	2010
Eutelsat KA-Sat	Europe, Mediterranean	82	2010
Hughes Echostar 17	North America	60	2012
OneWeb Constellation (LEO)	Global	720 Sat.	planned

geostationary orbit; however, O3b (medium Earth orbit - MEO) and the proposed OneWeb constellation (low Earth orbit - LEO) use lower orbits for relaxed link budgets. For mobile Internet on aircrafts and ships, coverage in remote areas is of great importance. Currently, only the three Inmarsat-5 satellites for the Global Xpress service offer quasi-worldwide coverage (except for the polar regions) and are, thus, a big milestone toward mobile Ka-band usage. Therefore, this service is chosen as reference for the further analysis. For mobile communications, the downlink frequency band from 19.7 to 20.2 GHz and the uplink band from 29.5 to 30 GHz are used. The spot beams feature left- and right-hand circular polarisation and two frequency bands to minimise interference in a four-colour arrangement. Thus, a mobile terminal must be dual-polarised and operate in both bands in order to work in all beams. Furthermore, a possible simultaneous usage of both polarisation (polarisation multiplexing) and frequency bands would allow a seamless handover from one spot beam to the next.

For a Ka-band ground terminal Tx, an equivalent isotropic radiated power (EIRP) of 50 dBW is in many cases sufficient for high-speed communications. In addition, it avoids some regulatory complications [19]. It requires large enough arrays or sufficiently powerful amplifiers, as exemplified in Table 2. Besides the EIRP in the main beam, the array beamwidth and side-lobe level has to comply with the respective standards to avoid interference with other satellites [20–22]. For arrays with a low number of controllable array elements (channels with a phased shifters or DBF circuitry), this can, in principle, be achieved by using adjusted elementary radiators with higher gain on an adapted grid. The drawback is a significant reduction in the possible scanning range, which is of major importance in the mobile context. The maximum possible scanning angle $\theta_{0,\,max}$ for a specific number of array elements is therefore also included in Table 2. To obtain a maximal grating lobe free scanning range, the arrays presented in this paper use an inter-element spacing of $\lambda_0/2$, where λ_0 is the free space wavelength. Thus, a 64×64 element array would yield an antenna size of 480×480 mm^2 at 20 GHz and 320×320 mm^2 at 30 GHz.

The Rx performance is dictated by noise. It can be improved by increasing the gain/size of the ground terminal or using a better low-

Table 2 EIRP in the main beam and scanning range for different array sizes and amplifier output powers P_A

	16×16	32×32	64×64	64×9
EIRP, $P_A = 0$ dBm	23.2 dBW	35.2 dBW	47.3 dBW	30.2 dBW
EIRP, $P_A = 10$ dBm	33.2 dBW	45.2 dBW	57.3 dBW	40.2 dBW
EIRP, $P_A = 20$ dBm	43.2 dBW	55.2 dBW	67.3 dBW	50.2 dBW
$\simeq \theta_{0,\,max}$	$\pm 15°$	$\pm 25°$	$\pm 45°$	$\pm 45°$ (one dimensional)

Table 3 Link budget analysis of different Rx-terminal sizes

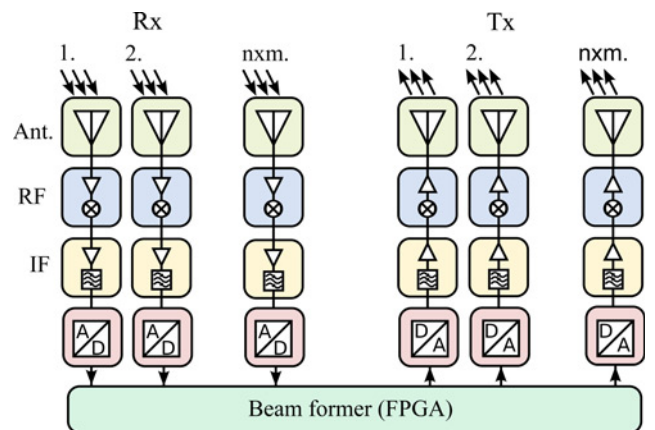|	16×16	32×32	64×64	64×9
G/T, dB/K	0.4	6.5	12.5	4
C/N	−6.6	−0.5	5.5	−3
spectrum efficiency, bps/Hz	–	0.75	1.8	–
data rate, Mbits/s	–	27.0	64.8	–

noise amplifier (LNA). Table 3 summarises the results of a link budget analysis carried out for differently sized Rx terminals and a geostationary satellite. Here, the transponder bandwidth and the satellite EIRP are set to 36 MHz and 50 dBW, respectively. The antenna noise temperature is estimated using [23]. No rain margin is included, since aircrafts mostly operate above the clouds. The frontend and antenna losses are assumed to be 3.0 dB, the noise figure of the LNA 2.0 dB, and its gain 30 dB. The array gain over the effective system temperature (G/T) is calculated according to [24] and depends strongly on the number of elements. Finally, the carrier-to-noise ratio (C/N) is calculated and turned into the downlink data rates achievable with DVB-S2 (Digital Video Broadcasting - Satellite - Second Generation) [25]. Since the standard requires C/N to be $>−2.4$ dB, values are specified for the 16×16 and 64×9 arrays. Operating smaller terminals would allow for very low data rates only. From Table 3, it is evident that a large aperture is of crucial importance in this respect.

2.2 System design

Fig. 1 depicts the block diagram of the overall system. The central unit is the beam former which consists of one or more field programmable gate arrays (FPGAs). These provide the computational power to process multiple channels in real time. The beam former is also the link between the separate Rxs (Rx, on the left) and Txs (Tx, on the right).

Rx and Tx are further subdivided into the antenna array, the radio frequency (RF) frontend, the intermediate frequency (IF) circuit, and the analogue-to-digital conversion (ADC) block. The RF block is comprised of a mixer, an image reject filter and either an LNA (Rx) or a (medium) power amplifier (Tx). The IF provides the high signal amplification and bandpass filtering that is necessary for satellite communication. The ADC and digital-to-analogue conversions are clocked at 56 MHz to enable an analogue bandwidth of up to 28 MHz. The used FPGA are from the Xilinx Virtex series [26, 27]. For polarisation multiplexing, each array element requires two complete processing chains – one for each polarisation.

Microwave monolithically integrated circuits (MMIC) do not scale well with frequency so that their integration in an array

Fig. 1 Schematic of a DBF array with central beam former and separate Rx and Tx apertures

becomes more complex at higher frequencies. To cope with these constraints, two different design approaches are pursued for the Rx and Tx RF frontends. The details are provided in Sections 3 and 4. As this contribution focuses on the great challenges associated with the complex frontend designs, details of ADC and baseband processing are not further addressed in the following. However, further information is available in [17, 26].

2.3 Digital beamforming

DBF compares favourably to phased arrays in terms of performance and RF circuit complexity. To make efficient use of this technique, all channels, i.e. all antenna elements, have to be processed in the analogue domain from the RF to the digital baseband creating a rather extensive circuitry. For each channel, further processing is required in digital domain. Beamforming, for instance, is performed by determining complex weighting coefficients and multiplying them with the complex baseband signal. Therefore, the complex weighting coefficients replace the phase shifters and variable attenuators used in phased arrays. In case of the Rx, a summation of all channels generates the final sum signal of the array. Further processing such as narrowband filtering might also be implemented in digital domain, which further increases the hardware performance requirements. The continual advancement of FPGA technology, however, eases these tasks. For this design, a Xilinx FPGA from the Virtex series is used [26].

DBF significantly reduces the number of required components and control circuits in the RF frontend. Instead of phase shifters and variable attenuators, a single mixer per channel suffices. In addition, at higher frequencies such as at Ka-band phase shifters are not widely available and introduce high losses. DBF also offers some other unique advantages. These include the capability of supporting multiple independent beams that enable instantaneous communications with several satellites. In a satellite scenario, this is specifically useful for communication with low Earth orbit satellites (e.g. OneWeb) or the spot beam handover in a geostationary scenario. Furthermore, the satellite position relative to the antenna can be determined without knowledge of the position and orientation of the terminal using direction of arrival (DOA) estimation. DOA algorithms such as ESPRIT (Estimation of Signal Parameters via Rotational Invariance Technique) [28] and MUSIC (Multiple Signal Classifier) [29] are well-known radar techniques. DOA is of particular importance on-board vehicles without precise navigation tools.

An important task during mobile use is tracking of the satellite direction. The tracking speed in a DBF system is mainly limited by the computational power of the beamformer. Thus, faster FPGA enables higher update rates. The same holds true for beam scanning, which is basically the same task as tracking. Since no inertia is involved in the scanning process, the achievable angular beam scanning velocity and acceleration is only limited by the update rate. With the available clock rates of FPGA in the high megahertz (MHz) range, scanning speed is thus in most configurations not a limiting factor of the approach.

As another major benefit, DBF enables a complete mutual coupling compensation of the antenna elements [30]. This greatly improves the overall system performance, because the smooth patterns of uncoupled elementary radiators can be restored and the cross-polar signal can be suppressed.

3 Receive terminal

3.1 Rx architecture

The Rx schematic is shown in Fig. 2. It consists of the antenna array, the RF frontend, and the IF stage. The signal at a centre frequency of 19.95 GHz at the antenna is amplified by an UMS CHA2090 LNA, filtered for a high image frequency rejection, and then downconverted to the IF at 1.855 GHz with the subharmonically pumped HMC337 mixer by Hittite. At this IF, cheap and widely available electronics for mobile communications can be employed. In a next step, the signal is converted to digital domain by a 56 MHz ADC.

At the IF, variable gain amplifiers (VGAs) and automatic gain control boost the signal-to-optimal ADC drive level. Surface acoustic wave filters with steep roll-off reduce the out-of-band noise. Fig. 3 shows a fabricated IF board with 16 parallel channels.

3.2 Array design

The radiating element used for the array design is closely investigated in [31]. It is based on a multilayer circular patch antenna with a ring feed to enable left- and right-hand circular polarisation required for the four-colour scheme of the satellite spot beams. To realise an active array based on a tile architecture with polarisation multiplexing, the available surface area is insufficient if a $\lambda_0/2$ element spacing is imposed. The reason is that for polarisation multiplexing two LNA and mixer MMICs have to be integrated per antenna. Therefore, an innovative approach using flex-rigid substrates is used to effectively double the available area beneath the
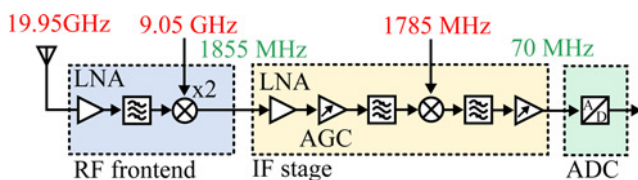

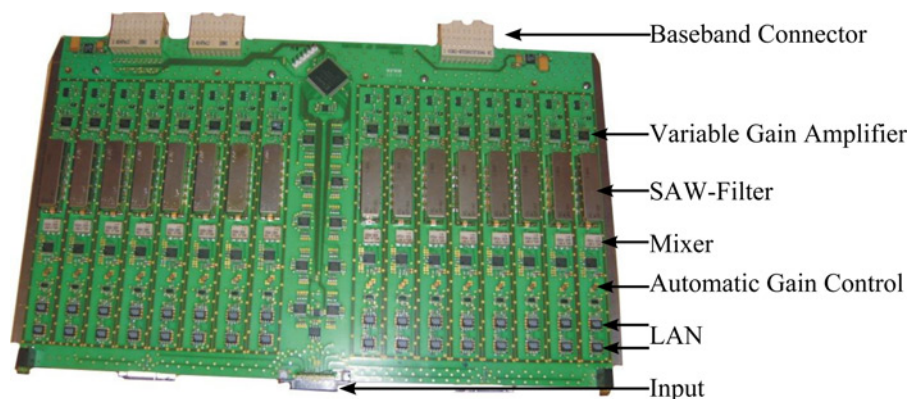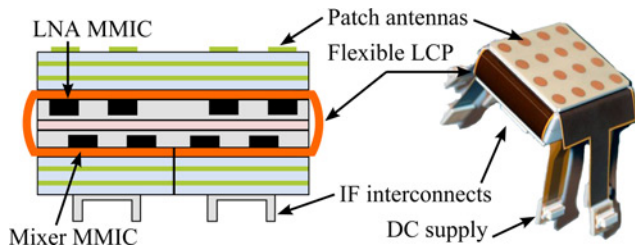**Fig. 2** *Schematic of a single DBF receive channel with frontend, IF, and baseband*

Fig. 3 *Fully equipped IF board with 16 channels*

Fig. 4 *Schematic and photograph of a 4 × 4 flex-rigid Rx-module*

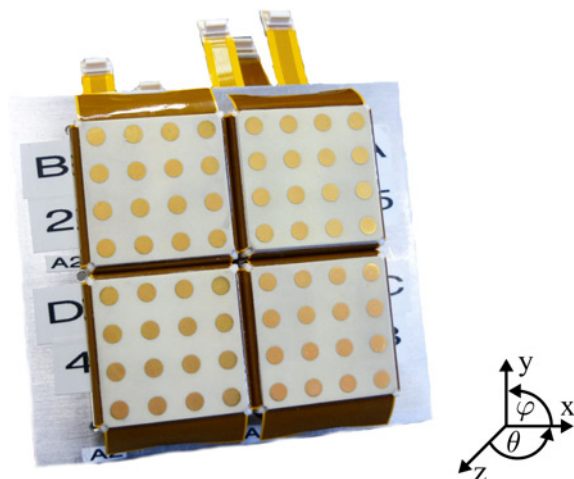**Fig. 6** *8 × 8 Rx array mounted on the manifold in an anechoic chamber*

antenna. The flexible part, a Rogers 3850 liquid crystal polymer substrate, is wrapped around the module to connect the upper and the lower layers of the arrangement. It also contains the image reject filters. The implementation of this design in the active 4 × 4 array with $\lambda_0/2$ element spacing shown in Fig. 4 was presented in [32]. Each active 4 × 4 array modules has a total weight of 26 g. The LNA MMIC is placed with minimal distance to the antenna to minimise the insertion loss.

In this contribution, a larger array consisting of four such modules is realised, thereby demonstrating the scalability of this approach. The achievable array size is not limited by the RF modules. However, in DBF systems the signal processing requirements increase with more antenna elements, making a realisation more challenging. Furthermore, thermal management in the backend becomes more involved with larger arrays and, thus, with more total consumed power.

Fig. 5 illustrates the array arrangement. The four modules are placed on a rectangular grid and fixed on a metal base plate. Arrays of arbitrary size are obtained by adding modules. The distance between modules is $13/20\lambda_0$, which violates the $\lambda_0/2$ requirement. It is dictated by the flexible substrate which can only be bent with a finite radius to avoid excessive mechanical stress. However, the scanning range of the array is limited by the patch radiation pattern to about 60°, so that grating lobes do not yet occur.

3.3 Measurement results

For the experiments, the 8 × 8 Rx array is mounted on a manifold which incorporates the IF channel distribution and the DC current supply. It also contains the heat exchanger for thermal management which collects the excess heat from the active antennas through heat pipes [32] and is subjected to liquid cooling. The liquid cooling system is chosen because of its simplicity but could be replaced by a heat pipe-based solution for usage on aircrafts with higher

requirements. Fig. 6 shows the total Rx arrangement with the four modules in the anechoic chamber during the far-field measurements. The manifold is covered with absorbing material to minimise reflections. The cables for the IF channels and DC supply, and the hoses for the coolant can be seen at the bottom. The far-field measurements are conducted using a high-quality dual-polarised circular horn antenna as a reference transmit antenna.

To obtain array patterns using a DBF receive array in a far-field measurement setup, a slightly different approach than with a phased array can be taken to allow for an advanced analysis. The hemisphere above the array is sampled at different angular positions. Here, a 1°-resolution in the elevation plane is chosen. At each position, a short period of the time-domain signal is sampled and recorded with the analogue-to-digital converters in every channel. This data can then be processed offline with DBF algorithms to determine the array characteristics.

The following results are obtained using DBF in combination with a standard calibration, i.e. with an elementwise normalisation of the magnitude and phase in bore-sight direction, and without any amplitude tapering (uniform array). If not otherwise noted, the results presented in the following are all obtained at the centre frequency of 19.95 GHz. Fig. 7 depicts the array pattern in the $\varphi = 0°$ plane at the centre frequency and at the band edges in comparison with the ideal case at the centre frequency with the beam scanned to $\theta_0 = 0°$. The ideal case is assumed to be the array factor multiplied

Fig. 5 *8 × 8 Rx array based on four modules mounted on a base plate and the used coordinate system*

Fig. 7 *Radiation patterns without beam scanning ($\theta_0 = 0°$) at corner and centre frequencies and the cross-polarisation in the $\varphi = 0°$ plane*

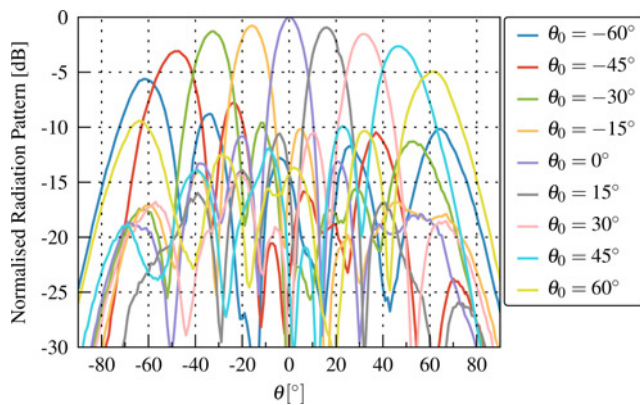**Fig. 8** *Pattern for different scanning angles in the φ = 0° plane*

by the uncoupled single radiator pattern. It can be seen that the power in the main beam slightly drops at the lower band edge. This is due to a shift of the antenna resonance. Both beamwidth and shape are in good agreement with the ideal case. The cross-polar isolation (XPI), i.e. the ratio of the received power at the same antenna polarisation port for co- and cross-polar excitations, exceeds 20 dB in the main beam and the highest side lobe is more than 10 dB below the peak. The lower than expected side lobe is caused by defective channels close to the array edges that effectively create an amplitude taper.

Fig. 8 illustrates the scanning range of the array in the φ = 0° plane. The amplitude is 3 dB down at about ±45° which is smaller than expected. This is mainly due to coupling effects which degrade the single element radiation pattern. It can be observed that grating lobes start to emerge when scanning close to $\theta_0 = 60°$, which is expected due to the irregular grid caused by the modules.

To demonstrate the DBF scanning ability for DOA detection, a Tx is placed at $\theta = 0°$, $\varphi = 0°$. The beam is then digitally scanned at a finite set of angles in the upper hemisphere and the total received signal level is determined. The scanning is performed by determining one complex weighting coefficient for each angle and channel and multiplying them with a short signal (2000 samples). The sum signal is then calculated for each coefficient.
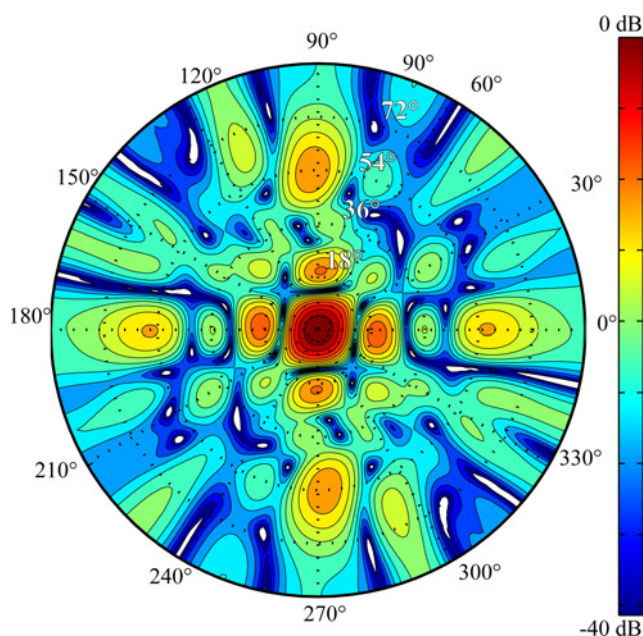

Fig. 9 *Target detection (DOA) by scanning the beam with a single Tx located at θ = 0, φ = 0*

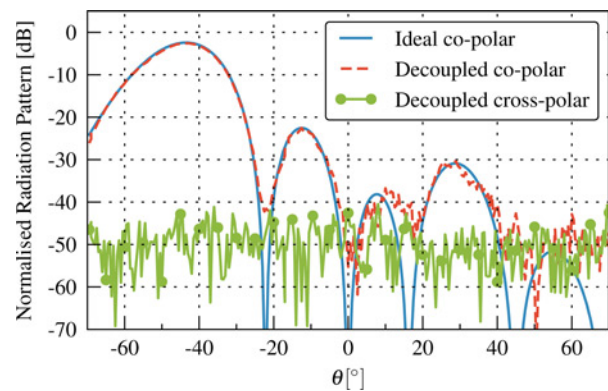Fig. 9 depicts the obtained results in a polar plot with the azimuth on the angular axis and the elevation on the radius.

A maximum appears in the centre, while several additional maxima can be observed that are caused by side lobes. For this method a single snapshot of the time-domain data is sufficient. The speed and angular discretisation of the scanning is only limited by the computational power of the used beamformer.

DBF allows for a compensation of the mutual coupling if the coupling matrix is known [33]. Coupling compensation smoothes the pattern of the elementary radiators, since they approach their ideal uncoupled shape. Furthermore, the cross-polarisation can be suppressed, which improves the link budget. During the measurements, enough data was collected to perform a decoupling of the co- and cross-polarised channels. The effectiveness of this approach is demonstrated by generating a pattern for a beam scanned at $\theta_0 = 45°$ in Fig. 10. The obtained pattern closely matches the ideal one and exhibits exceptional XPI.

The high XPI leads to an axial ratio (AR) close to 0 dB. The AR in the main beam is plotted in Fig. 11 for different scanning angles. It remains close to 0 dB throughout the scanning range and is much improved in comparison with the calibrated array.

The functionality of the thermal management is monitored with an infrared camera, which captures the antenna surface temperature. Each LNA dissipates about 250 mW and each mixer about 100 mW of thermal power. Thus, each active antenna dissipates 700 mW during dual-polarisation operation, which totals to about 11 W per module. When all 128 co- and cross-polar channels are turned on, one observes the temperature distribution shown in Fig. 12. The modules and patch antennas can clearly be distinguished. The temperature observed on the actual patch antennas is inaccurate, since the emissivity used for calibration of the infrared image is set for the substrate material and not for metal. The maximum temperature is 58°C and can be observed at the corners of the modules, while the areas along the horizontal centre axis are much cooler. The reason for this distribution is that the heat-spreader inside the module is mounted along this centre axis and
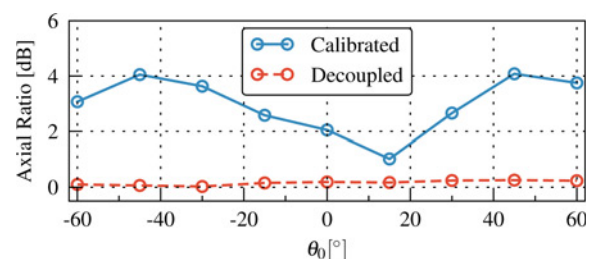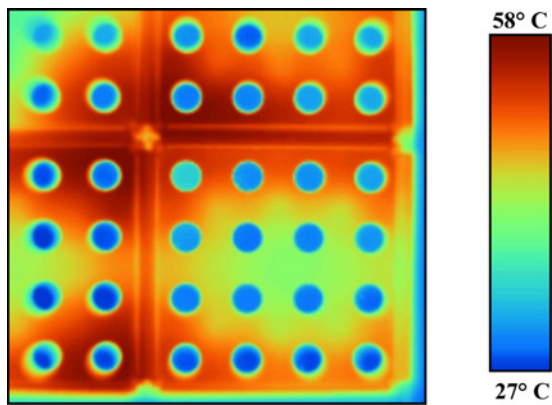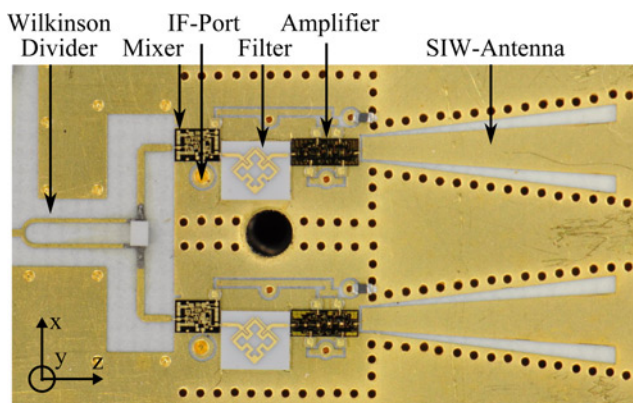

Fig. 10 *Decoupled co- and cross-polar antenna patterns for a 45°-scanning angle*

Fig. 11 *Axial ratio in the main beam of the calibrated and decoupled Rx array when scanned to different angles*

Fig. 12 *Thermal image of the Rx array when all channels are switched on (detail view)*

Fig. 13 *Two channels of a Tx frontend with SIW antenna and active circuitry*

hence provides better cooling. A temperature of 58°C is, however, uncritical for MMIC operation.

The proposed Rx array was experimentally verified in a field test on a mobile platform. The Rx terminal was integrated with a Tx provided by our project partner IMST GmbH [27] inside a roof rack box on a car. External modems were used for the data signal. Inside the FPGA, beamforming, scanning, and tracking was implemented, while DOA and decoupling were offloaded to an external computer. The car was then driven around a stationary transceiver tower that supplied an Internet connection to users inside the car. The feasibility of the taken approach was verified through this demonstration.
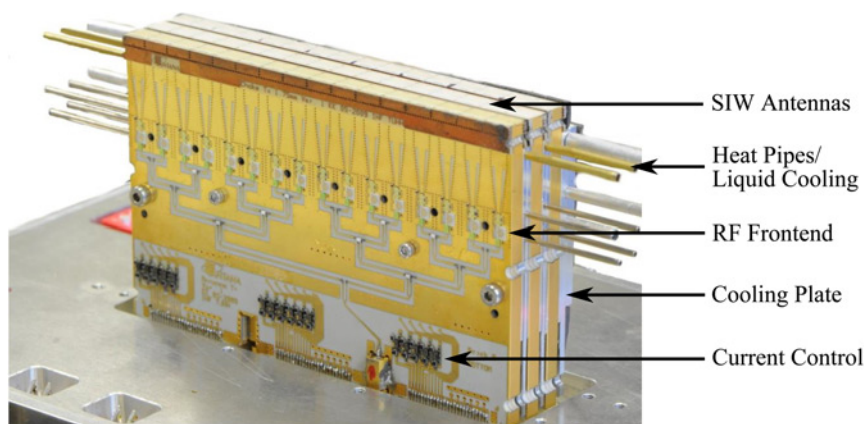
4 Transmit terminal

4.1 Array design

The integration of active circuitry for polarisation multiplexing in a $\lambda_0/2$-spaced antenna array is even more challenging at the higher transmit frequency of 30 GHz. Though the tile architecture offers very low-profile designs, the integration of MMICs on multiple layers would make the packaging and thermal management very complex. Therefore, a brick architecture is chosen [34] that trades low profile for available surface area. Since edge radiators in printed circuit board technology are required to construct a brick array, substrate integrated waveguide (SIW) horn antennas are utilised [35, 36]. The 16×1 active array is further discussed in [18] and the decoupling of the active array is demonstrated in [37].

The EIRP of Tx antennas in satellite communication systems has to comply with the respective standards [21, 22] to minimise interference with neighbouring satellites. The European Telecommunications Standard Institute (ETSI) and International Telecommunication Union (ITU) thus provide pattern masks that must not be exceeded. In an array setup, this is typically achieved using amplitude tapering in combination with a large enough antenna aperture. The arrays investigated in this paper are not large enough for a realistic satellite link, as their main purpose is to prove the feasibility of the approach. To comply with the provided masks, the transmit power in the main beam would be very low or different techniques not suited for satellite links such as spread spectrum would have to be used. Thus, amplitude tapering is not performed and no comparison with the pattern masks is shown. However, the modular design of the Tx allows for the construction of larger arrays that satisfy the needs and comply with regulation.

Fig. 13 shows two neighbouring channels on the top side of a module. The local oscillator (LO) signal is fed from the left to the Hittite HMC264 mixers through a Wilkinson power splitter. The IF is fed to the mixer through a via on the bottom. The upconverted signal is filtered, amplified by a 20 dBm output power Avago AMMC6232, and then radiated by the SIW antenna on the right. The amplifier is placed very close to the antenna to minimise the losses of the transition. According to Table 2, the output power is sufficient for a good link budget if used in an array setup. The total consumed DC power is 100 mW per mixer and 500 mW per amplifier. This sums up to 1.2 W per antenna element and to 19.2 W per module if polarisation multiplex is used. Neighbouring antenna elements have a different polarisation with the complementary channels for a multiplex placed on the bottom side of the module. Circular polarisation is realised by a septum polariser inside the SIW.

The modules are realised as linear 16-element arrays and weigh about 40 g. Larger entities are formed by stacking and juxtaposing identical modules. The array shown in Fig. 14 consists of three stacked modules mounted on a manifold. The aluminium cooling

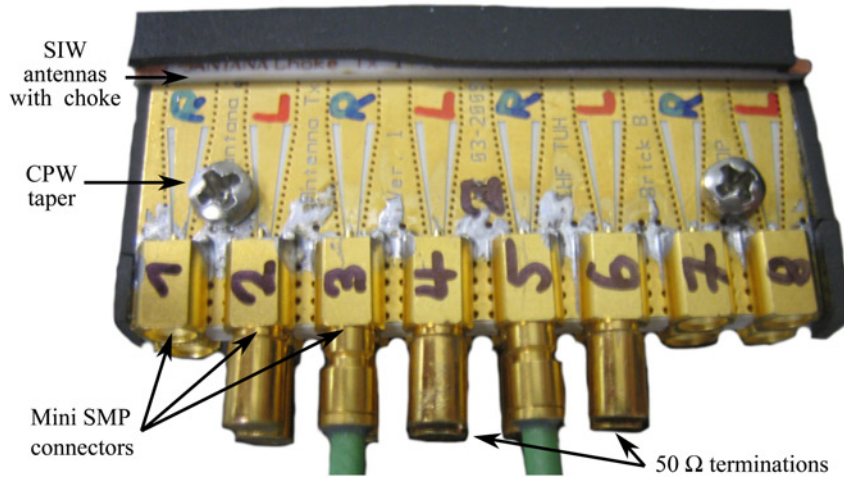**Fig. 14** *3 × 16 Tx array with front cooling plate removed*

Fig. 15 *Photograph of the 8 × 1 passive array [18]*

plates placed between them ensure the thermal management and at the same time provide mechanical protection for the subjacent chipsets and circuits. The front cooling plate has been removed so that the various components such as the SIW, the RF frontends, and the LO distribution become visible in the photograph. Pipes for coolant transport or heat pipes inserted in the cooling plates remove the excess heat. This approach is scalable in both dimensions and is only limited by the thermal conductivity and the available length of the heat pipes.

4.2 Measurement results

Measurements on the active array, i.e. the antennas with the RF frontends, are reported in [37]. In this contribution, the focus is on the passive SIW structure to assess its performance limits and relate them to the behaviour of the active array. Fig. 15 shows a photograph of a realised passive 8 × 1 antenna array. The antenna ports are accessed via Mini-SMP (Subminiature Push-On) connectors. Unused channels are terminated with 50 Ω coaxial loads.

In the following, only the right-hand circular polarised (RHCP) channels are reported since the left-hand ones (LHCP) behave similarly. The measurements are performed using a dual-polarised horn antenna as an Rx in an anechoic environment. Fig. 16 illustrates the radiation patterns of all eight elementary SIW antennas at 29.75 GHz for the case of a standard calibration. The cross-polar component is suppressed by only 10–20 dB.

This is mainly caused by mutual coupling. Indeed, when compensation is applied [30] the XPI is considerably improved as can

be seen in Fig. 17. In addition, the differences between the array elements are significantly reduced.

Fig. 18 shows the array radiation pattern for a uniform amplitude excitation and a simple calibration. The co-polarised pattern is very close to array theory and varies only slightly at higher elevation angles. The XPI reaches about 20 dB in the main beam and degrades at higher elevation angles. Coupling compensation again substantially improves this figure (Fig. 19). The remaining
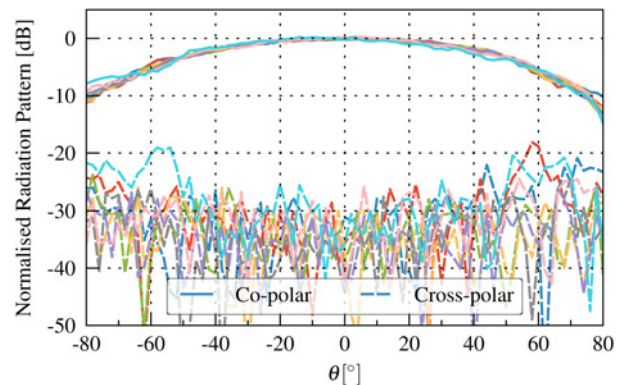

Fig. 17 *Decoupled RHCP co- and cross-polarised patterns of each antenna element at 29.75 GHz. One antenna is excited while the others are terminated with a matched load*
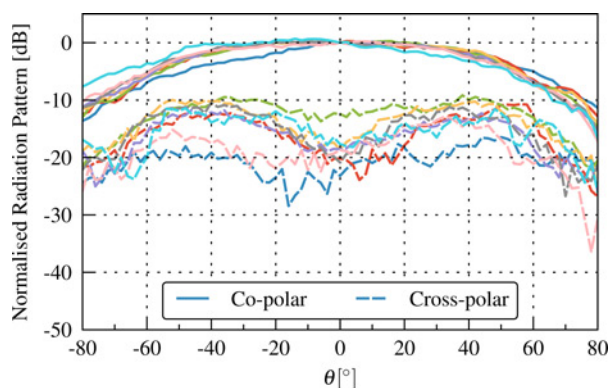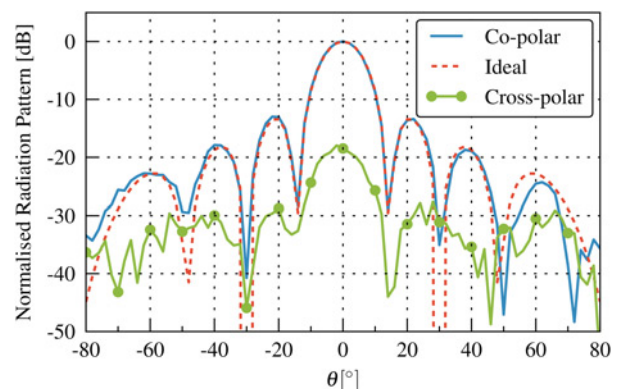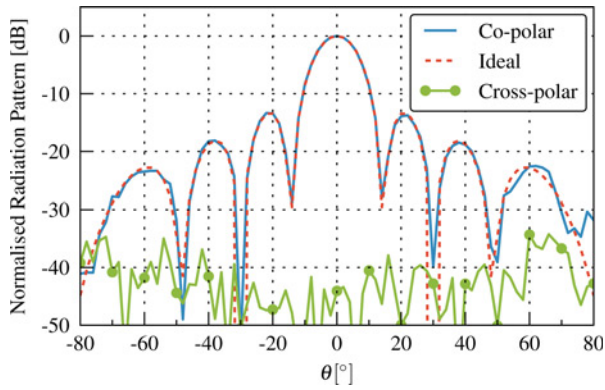

Fig. 16 *Calibrated RHCP co- and cross-polarised patterns of each antenna element at 29.75 GHz. One antenna is excited while the others are terminated with a matched load*

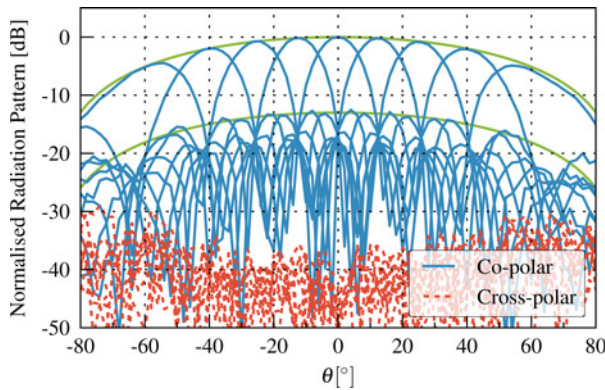**Fig. 18** *Radiation pattern of the calibrated passive 8 × 1 RHCP array at 29.75 GHz*

Fig. 19 *Radiation pattern of the decoupled passive 8 × 1 RHCP array at 29.75 GHz*

Fig. 22 *Radiation pattern of the decoupled 16 × 1 active array at 29.75 GHz*
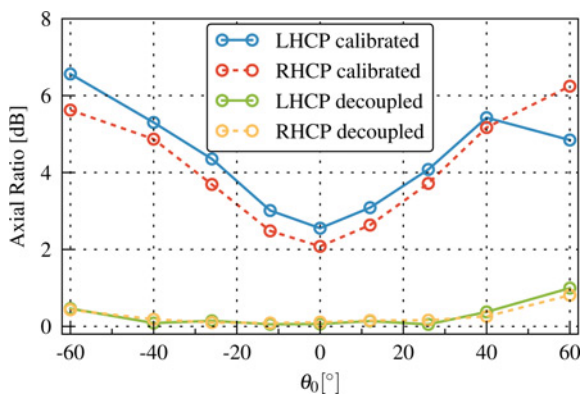
differences in the co-polar component at higher angles most likely stem from reflections during the far-field measurement.

Fig. 20 presents the decoupled radiation pattern when scanning the beam to different angles θ_0. The two plotted envelope curves indicate the maximum possible gain and side-lobe level as determined from the single antenna radiation characteristic. Beyond $\theta_0 = 40°$ the gain drops significantly and the beam widens. The XPI remains high throughout the whole scanning range.
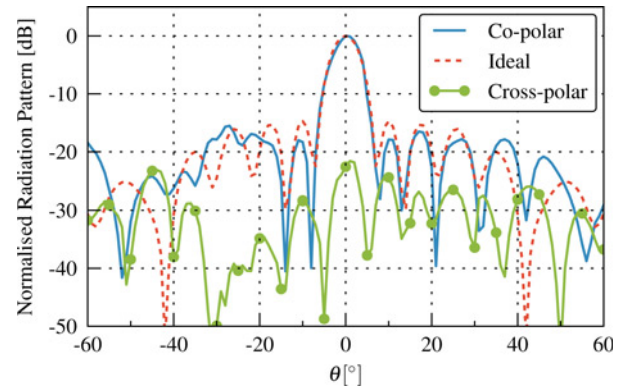
The AR in main beam direction is derived from the co- and cross-polar patterns. The results for both RHCP and LHCP are compiled in Fig. 21 at different scanning angles θ_0. The AR of the calibrated array depends on the average AR of the antenna elements. Decoupling leads to a significant improvement. The AR remains

Fig. 20 *Radiation pattern of the decoupled passive 8 × 1 RHCP for different scanning angles*

Fig. 21 *Axial ratio in the main beam of the calibrated and decoupled 8 × 1 Tx array when scanned to different angles*

below 1 dB over the complete scanning range. This is important with respect to the strict limits imposed on beamwidth, side-lobe level, and AR by regulation (e.g. [20]).

Fig. 22 reports the results obtained when decoupling the active array. More information is provided in [37]. Obviously, the coupling compensation is also very beneficial here, though not quite as effective as in the passive case. The ideal case, i.e. the array factor multiplied with the pattern of an uncoupled SIW-antenna, and the measured co-polar pattern are in good agreement. The XPI is better than 20 dB, which corresponds to an AR of <1 dB.

5 Conclusions

A modular array system for ground-based mobile satellite communication at Ka-band (ESOMP) consisting of separate receive and transmit units is presented. The antennas feature DBF and full polarisation multiplexing capability. This enables the terminals to be used with the four-colour scheme employed by modern Ka-band HTS. Furthermore, DBF techniques such as DOA estimation and coupling compensation enable high performance and flexible use of the proposed array system.

As demonstrated in this contribution, the modular design approach allows for a flexible extension to larger arrays. In principle, it is thus suitable to realise the array sizes required for high-speed satellite links.

The proposed innovative Tx and Rx designs, though relying on standard printed circuit technology, allow for the high integration densities needed for polarisation multiplexing at Ka-band and even beyond. Extensive measurements validate the feasibility of the approach. In addition, they demonstrate the huge benefits of DBF regarding, for instance, its inter-element coupling compensation ability which leads to almost ideal performance characteristics.

6 Acknowledgments

7 References

[1] I. International Telecommunication Union: 'The world in 2013 ICT facts and figures', Geneva, Switzerland, 2013. Available at http://www.itu.int/en/ITU-D/Statistics/Documents/facts/ICTFactsFigures2013-e.pdf

[2]   Iridium Communications Inc. Itasca, Illinois, USA. Available at http://www.iridium.com

[3]   Inmarsat plc. London, England, UK. Available at http://www.inmarsat.com

[4]   Intelsat S.A. Luxembourg, Luxembourg. Available at http://www.intelsat.com

[5]   SES S.A., Société Européenne des Satellites. Betzdorf, Luxembourg. Available at http://www.ses.com

[6]   Appel K.I., Haken W.: 'Every planar map is four colorable', in Contemporary Mathematics (American Mathematical Society, Providence, RI, USA, 1989), vol. 98

[7]   Tooway by SES S.A., Société Européenne des Satellites. Paris, France. Available at http://www.tooway.com/

[8]   Moskvitch K.: 'In-flight Internet to take off?', BBC, May 2012. Available at http://www.bbc.co.uk/news/technology-18021468

[9]   Hotten R.: 'Budget long-haul flights 'can work'', BBC, June 2013. Available at http://www.bbc.co.uk/news/business-22840790

[10]   C2SAT communications AB. Stockholm, Sweden. Available at http://www.c2sat.com/

[11]   EPAK GmbH. Dresden, Germany. Available at http://www.epak.de/

[12]   Stark A., Jacob A.F.: 'Complex loads for millimeter-wave digital phase shifter design'. 2011 European Microwave Integrated Circuits Conf. (EuMIC), October 2011, pp. 462–465

[13]   Lambard T., Lafond O., Himdi M., ET AL.: 'Ka-band phased array antenna for high-data-rate SATCOM', *IEEE Antennas Wirel. Propag. Lett.*, 2012, **11**, pp. 256–259

[14]   Sazegar M., Zheng Y., Maune H., ET AL.: 'Low-cost phased-array antenna using compact tunable phase shifters based on ferroelectric ceramics', *IEEE Trans. Microw. Theory Tech.*, 2011, **59**, (5), pp. 1265–1273

[15]   Rengarajan S., Zawadzki M., Hodges R.: 'Design, analysis, and development of a large Ka-band slot array for digital beam-forming application', *IEEE Trans. Antennas Propag.*, 2009, **57**, (10), pp. 3103–3109

[16]   Holzwarth S., Jacob A.F., Dreher A., ET AL.: 'Active antenna arrays at Ka-band: status and outlook of the SANTANA project'. 2010 Proc. Fourth European Conf. on Antennas and Propagation (EuCAP), April 2010, pp. 1–5

[17]   Geise A., Jacob A.F., Kuhlmann K., ET AL.: 'Smart antenna terminals for broadband mobile satellite communications at Ka band'. Second Int. ITG Conf. on Antennas, 2007. INICA'07, March 2007, pp. 199–204

[18]   Kuhlmann K., Jacob A.F.: 'Active 30 GHz antenna array for digital beamforming and polarization multiplexing'. 2010 IEEE MTT-S Int. Microwave Symp. Digest (MTT), May 2010, pp. 1276–1279

[19]   Eutelsat Communications: 'TOOWAY VSATs RF performance – type approval and characterization', 2014. Available at http://www.eutelsat.com/files/contributed/support/pdf/RF_Characterisation_Tooway.pdf

[20]   European Telecommunications Standards Institute, ETSI: 'Satellite Earth stations and systems (SES); harmonized EN for satellite interactive terminals (SIT) and satellite user terminals (SUT) transmitting towards satellites in geostationary orbit in the 29.5 GHz to 30.0 GHz frequency bands (ETSI EN 301 459 V1.4.1)' (European Telecommunications Standards Institute Std., 2007), June. Available at http://www.etsi.org/deliver/etsi_en/301400_301499/301459/01.04.01_60/en_301459v010401p.pdf

[21]   European Telecommunications Standards Institute, ETSI: 'Satellite Earth stations and systems (SES); harmonized EN for Earth stations on mobile platforms (ESOMP) transmitting towards satellites in geostationary orbit in the 27.5 GHz to 30.0 GHz frequency bands covering the essential requirements of article 3.2 of the R&TTE directive (Draft ETSI EN 303 978 V1.1.0)' (European Telecommunications Standards Institute Std., 2012). Available at https://www.etsi.org/deliver/etsi_en/303900_303999/303978/01.01.00_20/en_303978v010100c.pdf

[22]   I. International Telecommunication Union: 'Reference radiation pattern of earth station antennas in the fixed-satellite service for use in coordination and interference assessment in the frequency range from 2 to 31 GHz (Recommendation ITU-R S.465-6)' (International Telecommunication Union Std., 2010), January. Available at http://www.itu.int/dms_pubrec/itu-r/rec/s/r-rec-s.465-6-201001-i!!pdf-e.pdf

[23]   Dijk J., Jeuken M., Maanders E.: 'Antenna noise temperature', *Proc. Inst. Electr. Eng.*, 1968, **115**, (10), pp. 1403–1410

[24]   Lee J.: 'G/T and noise figure of active array antennas', *IEEE Trans. Antennas Propag.*, 1993, **41**, (2), pp. 241–244

[25]   European Telecommunications Standards Institute, ETSI: 'Digital video broadcasting (DVB); second generation framing structure, channel coding and modulation systems for broadcasting, interactive services, news gathering and other broadband satellite applications (DVB-S2) (ETSI EN 302 307 V1.3.1)' (European Telecommunications Standards Institute Std., 2013), March. Available at http://www.etsi.org/deliver/etsi_en/302300_302399/302307/01.03.01_60/en_302307v010301p.pdf

[26]   Geise A., Jacob A., Kuhlmann K., ET AL.: 'THE SANTANA PROJECT'. First CEAS European Air and Space Conf., 2007, Berlin, Germany, September 2007, pp. 1–4

[27]   Holzwarth S., Litschke O., Simon W., ET AL.: 'Highly integrated 8 × 8 antenna array demonstrator on LTCC with integrated RF circuitry and liquid cooling'. Fourth European Conf. on Antennas and Propagation, 2010. EuCAP 2010, April 2010, pp. 1–4

[28]   Roy R., Kailath T.: 'ESPRIT-estimation of signal parameters via rotational invariance techniques', *IEEE Trans. Acoust. Speech Signal Process.*, 1989, **37**, (7), pp. 984–995

[29]   Schmidt R.: 'Multiple emitter location and signal parameter estimation', *IEEE Trans. Antennas Propag.*, 1986, **34**, (3), pp. 276–280

[30]   Kuhlmann K., Jalas D., Jacob A.F.: 'Mutual coupling in Ka-band antenna array with polarization multiplexing'. Proc. 39th European Microwave Conf., Rome, Italy, September/October 2009, pp. 1–4

[31]   Geise A., Jacob A.F.: 'A ring-coupled patch antenna for broadband polarization multiplex at Ka-band'. Third European Conf. on Antennas and Propagation, 2009. EuCAP 2009, March 2009, pp. 1260–1263

[32]   Geise A., Jacob A.F.: 'Flex-rigid architecture for active millimeter-wave antenna arrays'. IEEE MTT-S Int. Microwave Symp. Digest, 2009. MTT'09, June 2009, pp. 809–812

[33]   Steyskal H., Herd J.: 'Mutual coupling compensation in small array antennas', *IEEE Trans. Antennas Propag.*, 1990, **38**, (12), pp. 1971–1975

[34]   Sanzgiri S., Bostrom D., Pottenger W., ET AL.: 'A hybrid tile approach for Ka band subarray modules', *IEEE Trans. Antennas Propag.*, 1995, **43**, (9), pp. 953–959

[35]   Kuhlmann K., Rezer K., Jacob A.F.: 'Circularly polarized substrate-integrated waveguide antenna array at Ka-band'. 2008 German Microwave Conf. (GeMIC), March 2008, pp. 1–4

[36]   Kuhlmann K., Rezer K., Jacob A.F.: 'Far field measurement on Ka-band substrate-integrated waveguide antenna array with polarization multiplexing'. 2008 IEEE MTT-S Int. Microwave Symp. Digest, June 2008, pp. 1337–1340

[37]   Kuhlmann K., Rohrdantz B., Jacob A.F.: 'Performance assessment and optimization of an active Ka-band antenna array with polarization multiplexing'. Accepted at the European Microwave Conf., Rome, Italy, October 2014, pp. 1–4